Nuclear Engineering and Technology 50 (2018) 1330–1338

Contents lists available at ScienceDirect

Nuclear Engineering and Technology

journal homepage: www.elsevier.com/locate/net

Original Article

Effects of sizes and mechanical properties of fuel coupon on the rolling simulation results of monolithic fuel plate blanks

Xiangzhe Kong [a], Shurong Ding [a, *], Hongyan Yang [b], Xiaoming Peng [b]

[a] Institute of Mechanics and Computational Engineering, Department of Aeronautics and Astronautics, Fudan University, Shanghai 200433, PR China
[b] Science and Technology on Reactor Fuel and Materials Laboratory, Nuclear Power Institute of China, Chengdu 610213, PR China

ARTICLE INFO

Article history:
Received 8 February 2018
Received in revised form
10 July 2018
Accepted 30 July 2018
Available online 31 July 2018

Keywords:
Numerical simulation
UMo/Zr monolithic fuel plate
Co-rolling simulation
Composite blank
Size and mechanical property

ABSTRACT

High-density UMo/Zr monolithic nuclear fuel plates have a promising application prospect in high flux research and test reactors. The solid state welding method called co-rolling is used for their fabrication. Hot co-rolling simulations for the composite blanks of UMo/Zr monolithic nuclear fuel plates are performed. The effects of coupon sizes and mechanical property parameters on the contact pressures between the to-be-bonded surfaces are investigated and analyzed. The numerical simulation results indicate that 1) the maximum contact pressures between the fuel coupon and the Zircaloy cover exist near the central line along the plate length direction; as a whole the contact pressures decrease toward the edges in the plate width direction; and lower contact pressures appear at a large zone near the coupon corner, where de-bonding is easy to take place in the in-pile irradiation environments; 2) the maximum contact pressures between the fuel coupon and the Zircaloy parts increase with the initial coupon thickness; after reaching a certain thickness value, the contact pressures hardly change, which was mainly induced by the complex deformation mechanism and special mechanical constitutive relation of fuel coupon; 3) softer fuel coupon will result in lower contact pressures and form interfaces being more out-of-flatness.

1. Introduction

Owing to having a high uranium density, UMo monolithic nuclear fuel plates have an attractive prospect to be used in advanced research and test reactors [1,2]. Nowadays, hot-isostatic pressure (HIP) and co-rolling [3–5] are regarded as two effective ways to manufacture monolithic fuel plates.

For co-rolling, four parts are firstly assembled together and then welded at the edges to form a composite blank, in which two covers and a frame are made of Zircaloy and UMo alloy is selected as the material for the fuel coupon. After multi-pass hot and cold rolling processes, the UMo coupon is expected to be bonded with the Zircaloy covers and frame [6,7]. After fabrication, the fuel coupon becomes a fuel meat, and the bonded covers and frame constitute the cladding of monolithic fuel plates. The co-rolling fabrication is a kind of solid state welding method.

The in-pile performances of UMo/Zr monolithic nuclear fuel plates are directly dependent on the bonding strength of the interface between the Zircaloy cladding and UMo fuel meat. A weak-bonded plate would easily result in interfacial failure in the reactor irradiation environments. The fission gases will then be released into the formed free volume, and surface blisters will take place at high burnup to threaten the service safety of fuel plates.

The bonding strength of fuel plates depends upon several manufacturing factors [8–13] such as the rolling temperature, the rolling speed, the reduction set-in-advance and so on. Besides, in order to achieve enhanced interfacial bonding strength, the UMo fuel coupon is generally set thicker than the frame part. Higher initial coupon thickness may result in heightened contact pressures between the fuel coupon and the other parts. According to the rolling-bonding theory, the contact pressures between the to-be-bonded surfaces should be high enough to achieve high bonding strength after hot-rolling [8,9]. So, the influence of the initial UMo coupon thickness on the contact pressures should be precisely investigated in order to optimize the structure of the composite blank. Owing to the fact that the elastic modulus and yield strength of UMo alloy will change with the mass fraction of Mo, so the resulted different mechanical properties of UMo will affect the mechanical interaction between the fuel coupon and the other

* Corresponding author.
E-mail address: dingshurong@fudan.edu.cn (S. Ding).

https://doi.org/10.1016/j.net.2018.07.019

parts during co-rolling. As a result, the effects of mechanical property parameters of fuel coupon should also be studied in order to select suitable UMo materials for monolithic fuel plates. Because it is both expensive and time consuming for structural optimization and material selection schemes with the traditional trial and error method, it would be an important way to perform finite element analysis for the co-rolling process.

Being a problem with multi-nonlinearities, an explicit finite element method should be adopted to calculate the displacement, strain and stress fields [14–17] for the co-rolling process. It is known that the composite blank for monolithic fuel plates would experience large deformation. Also, complex contact relations appear between the roller and the cover, but also among all the to-be-bonded parts. Besides, under the rolling temperature of 600–800 °C, the material of the cover and frame, Zircaloy, has a strain-rate-dependent mechanical constitutive relation [18]. All these complexities should be considered in the FEM simulation. Research is limited on the numerical simulation analysis of the co-rolling process for the composite blank of monolithic fuel plates. Comprehensive studies should be implemented.

In this study, a user material subroutine previously developed by us [20] is used to define the strain-rate-dependent mechanical constitutive relation of Zircaloy. FEM simulation of co-rolling process for the composite blank of monolithic nuclear fuel plates is carried out. The influences of the initial thickness and mechanical property parameters of the fuel coupon on the coupon deformation and the contact pressures between the coupon and the other parts will be analyzed.

2. Material properties and FEM models

In this study, the mechanical properties of Zircaloy are given as

$$E = \left[9.900 \times 10^5 - 566.9 \times (T - 273.15)\right] \times 9.8067 \times 10^4 \tag{1}$$

$$\nu = 0.3303 + 8.376 \times 10^{-5}(T - 273.15) \tag{2}$$

where E is the Young's modulus in Pa; ν depicts the Poisson's ratio; and T is the temperature in K.

The strain-hardening curve of Zircaloy is described as [18]

$$\sigma = K\varepsilon^n \left(\frac{\dot{\varepsilon}}{10^{-3}}\right)^m \tag{3}$$

$$K = \exp\left(8.755 + \frac{8663}{T}\right) \tag{4}$$

$$n = 0.027908 \tag{5}$$

$$m = -6.47 \times 10^{-2} + 2.203 \times 10^{-4} T \tag{6}$$

where σ is the true stress in Pa; ε and $\dot{\varepsilon}$ denote the true strain and true strain rate. If $\dot{\varepsilon} < 10^{-5}/s$, $\dot{\varepsilon} = 10^{-5}/s$. K, n and m refer to the strength coefficient in Pa, the strain-hardening exponent and the strain rate sensitivity exponent, respectively. A three-dimensional stress-update algorithm was developed [19,20] for this strain-rate dependent mechanical constitutive relation. In this study, the corresponding user-defined subroutine is used for the co-rolling simulation.

For the U-10Mo alloy, an ideal elastic-plastic model was taken into consideration [2]. The Young's modulus of 65GPaand the Poisson's ratio of 0.35 are adopted. The yield strength is 31.95 MPa under the co-rolling temperature of 1000 K.

The geometric sizes and process parameters are shown in Table 1. To study the influence of initial coupon thickness on the rolling simulation results, four cases are calculated with the initial thickness of the U-Mo coupon set as 1.15 mm, 1.20 mm, 1.25 mm and 1.30 mm, respectively.

Considering the symmetry in the structure and loading, a 1/4 part of the composite blank and rollers is built as the geometric model for rolling simulation, as shown in Fig. 1. The frame and the cover are bonded with each other at the zone depicted in Fig. 1 (b). The contact boundary conditions are respectively set to obey the Coulomb friction model between the roller and the cover, between the cover and the frame, between the cover and the coupon, and between the frame and the coupon. The rolling temperature is set as 1000 K.

Each case is simulated with the same roller rotational speed of 4 rad/s, and the same roll gap of 5.36 (2.68 × 2) mm.

Compared to Zircaloy and U-Mo alloy, the stiffness of the roller is much larger so that it is simplified as a rigid body in this study. An 8-node linear brick reduced integration element C3D8R is adopted for discretization of the considered geometric model. The finite element mesh can be found in Fig. 1 (c), and the total element number is 197691.

3. Results and discussion

Four cases considering different values of initial coupon thickness have been simulated, and the effects of initial coupon thickness on the contact pressures between the coupon and the other parts will be discussed. Considering that the mechanical properties of different U-Mo alloys vary with their constituents, lowered elastic modulus and yield strength of fuel coupon are used to obtain the rolling simulation results in Section 3.2. So, in this section the effects of coupon mechanical properties will also be investigated.

3.1. The influences of initial U-10Mo coupon thickness

For prediction of the metallurgical bonding strength between the U-10Mo fuel meat and Zircaloy cladding, the maximum contact pressures between the coupon and the cover are obtained. The contour plot of the maximum contact pressure at the upper surface of the U-10Mo coupon is shown in Fig. 2, which illustrates the results for the case with an initial coupon thickness of 1.20 mm. Here, the maximum contact pressure refers to the maximum value that every node has experienced during the whole rolling process.

It can be seen from Fig. 2 that the maximum value occurs at the region close to the central line, and the maximum contact pressure

Table 1
Model parameters.

Parameters	Value
Roller	
diameter (mm)	200
length (mm)	100
Zircaloy cover	
initial length (mm)	47
initial width (mm)	35
initial thickness (mm)	2.7
Zircaloy frame	
initial length (mm)	47
initial width (mm)	35
initial thickness (mm)	1.1
U-Mo coupon	
initial length (mm)	19.5
initial width (mm)	19.5

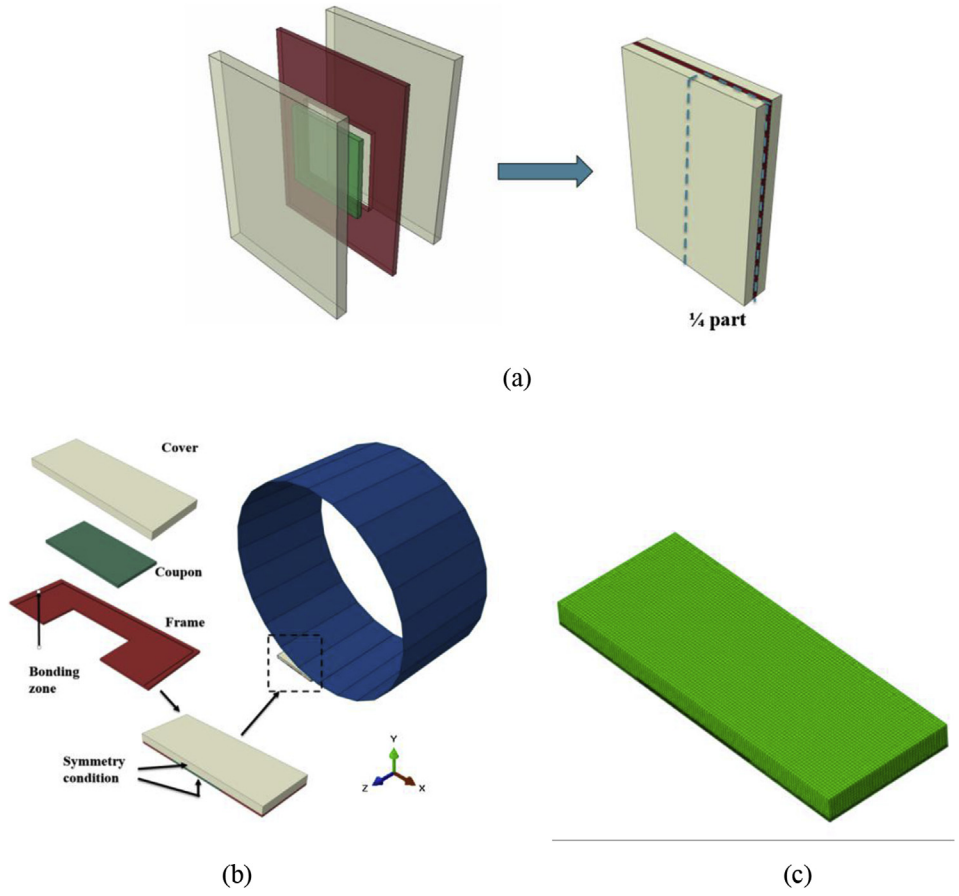

Fig. 1. a) The composite blank, b) the considered geometric model and (c) the mesh grid.

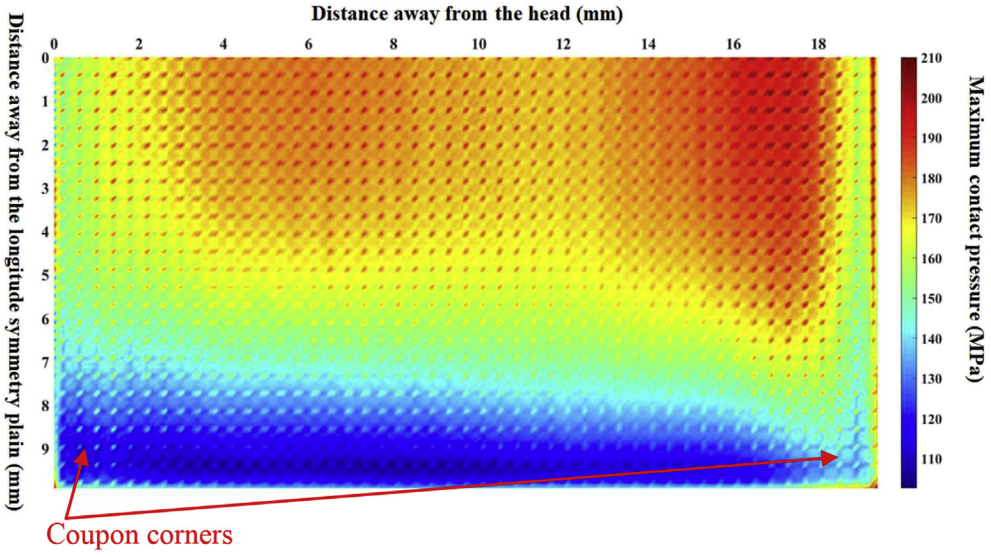

Fig. 2. The maximum contact pressure during rolling at the upper surface of the U-10Mo coupon.

decreases along the width direction as a whole. One can also find that the minimum contact pressure appears close to the edge in the width direction, being with a distance away from this edge, which means that the bonding strength might be weaker at this location. The contact pressures are smaller at a comparable large zone near the coupon corner, which enters into the roller gap earlier. While the contact pressures become higher at the other coupon corner in Fig. 2. According to the UT test [7], de-bonding really happened at the meat corners, as depicted in Fig. 3(a), which could prove the effectiveness of our simulation.

From Fig. 2 it can be also observed that the contact pressures at the coupon surface present some fluctuation, especially at the front

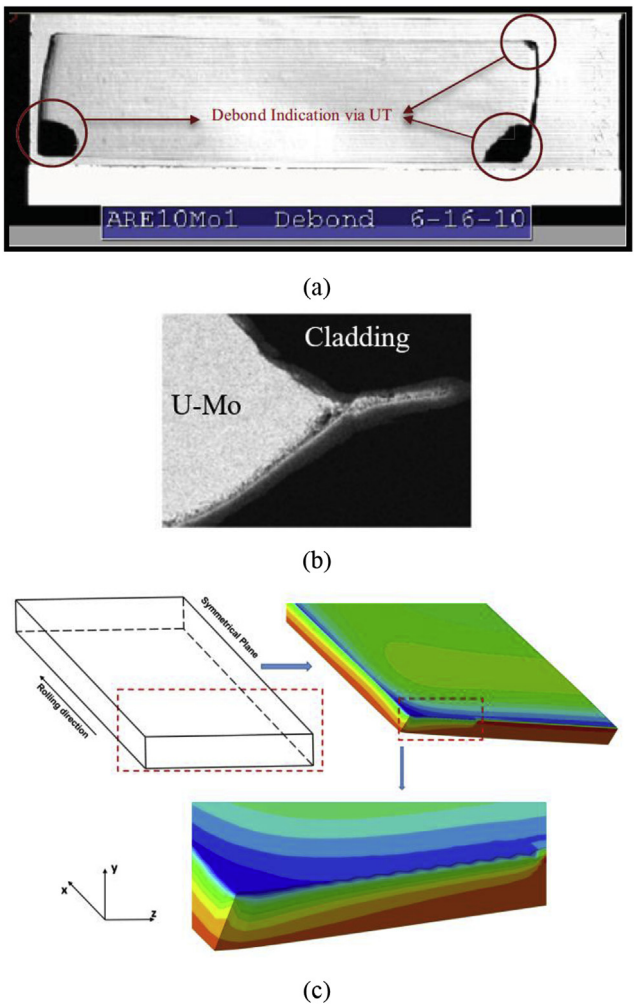

Fig. 3. (a) Plate UT image [7], (b) part of the deformed fuel coupon squeezed into the gap between the deformed cover and frame [7] and (c) the deformed fuel coupon in FEM simulation.

and back edges. The fluctuation mainly results from the velocity fluctuation of the composite blank during the kinetic process together with the complicated deformation patterns in the vicinities of the edges, and the contact state between the fuel coupon and the other parts is of complexity, especially for the fact that the thickness of the fuel coupon is higher than the frame part.

One can see from the UT image in Fig. 3(b) that due to existence of an initial gap between the frame and the cover (because of the thickened fuel coupon), a part of fuel coupon would be squeezed into this gap during rolling process. Similar phenomenon can be found in the numerical simulation, which will also lead to the complex distribution of contact pressures. Fig. 3(c) depicts the tail shape of the fuel coupon after rolling. It can be found that a wave-like shape emerges, which can demonstrate the fluctuation of the maximum contact pressures during co-rolling.

A path shown in Fig. 4 is selected to study the influence of the initial coupon thickness on the mechanical interaction between the coupon and the cover. The distribution of the maximum contact pressures and the actual through-thickness displacements along this path are given in Fig. 5.

One can find from Fig. 5 (a) that the maximum contact pressures along the output path generally tend to increase with the initial coupon thickness. However, the results of 1.25 mm-case and 1.30 mm-case are almost the same. The maximum values of 1.15 mm-case and 1.20 mm-case are 186.784 MPa and 213.148 MPa, respectively. They locate near the tail of the coupon. While the maximum contact pressures of 1.25 mm-case and 1.30 mm-case are about 100 MPa higher, and occur near the front end. With an increase of 0.05 mm from 1.20 mm, the maximum contact pressures during co-rolling rise evidently. It can be predicted that the bonding strength can be improved heavily.

From Fig. 5 (b), it can be found that for 1.25 mm-case and 1.30 mm-case, apparent dog-bone areas appear. One can find that near the tail end of the deformed fuel coupon the reduction is far less than the front end. The presented shape of the fuel coupon after co-rolling is closely related to the rolling direction. The coupon is squeezed towards the tail end during the co-rolling process, and at the tail end the coupon will be restrained by the frame, so a shape of dog-bone forms. With different initial thicknesses, it can be obtained that the current thicknesses of the fuel zone for the 1.25 mm-case and 1.30 mm-case exist larger differences, with some locations thicker than those for 1.15mm/1.20 mm cases and some regions thinner. As mentioned in Section 2, the numerical simulation results are obtained with the same roller gap. According to the results in Fig. 5(a) and (b) it can be known that an optimized roller gap should be designed in order to improve the interfacial strength and avoid large dog-bone-like deformation simultaneously.

From Fig. 5(c) it can be seen that the equivalent plastic strains of the cover for the 1.25mm/1.30 mm cases rise heavily, compared to 1.20 mm-case. The equivalent plastic strains are especially similar for 1.25 mm-case and 1.30 mm-case, which partly explains the reason for the similarity of the contact pressures for these two cases. In fact, this is basically induced by the complex deformation

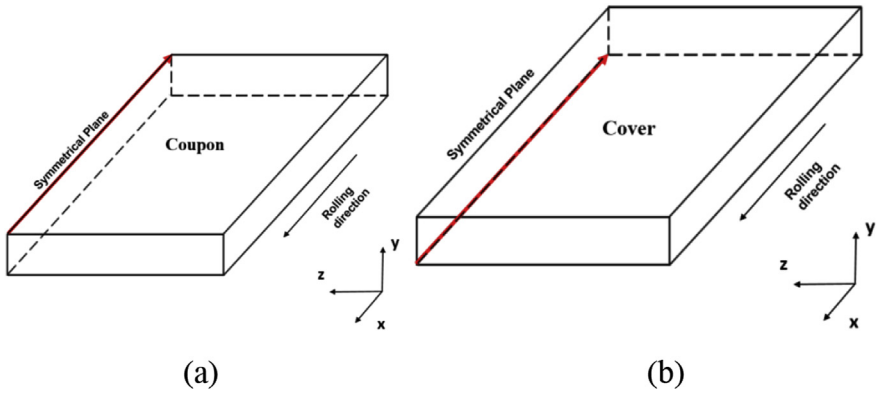

Fig. 4. The path along the longitudinal symmetrical plane of a) the fuel coupon and b) the cover.

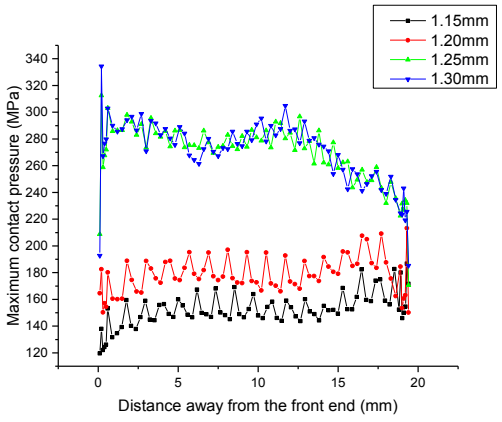

(a)

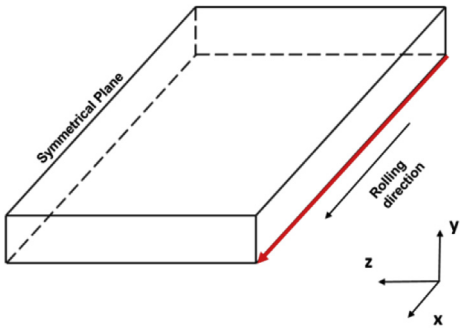

(a)

Fig. 6. The path along the lateral side of the fuel coupon.

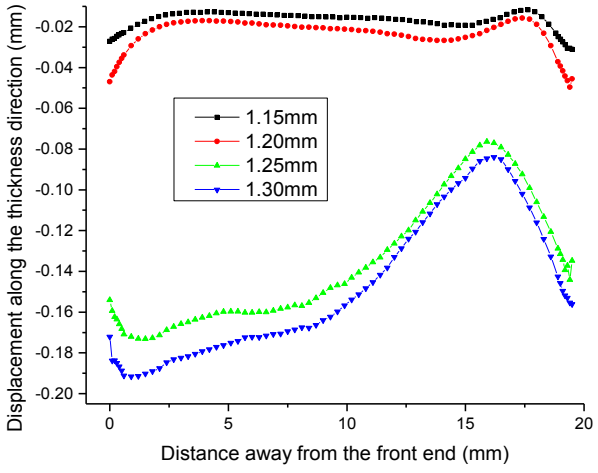

(b)

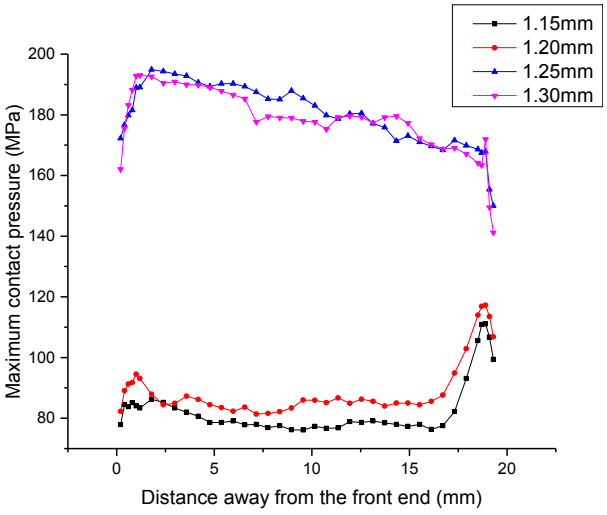

(a)

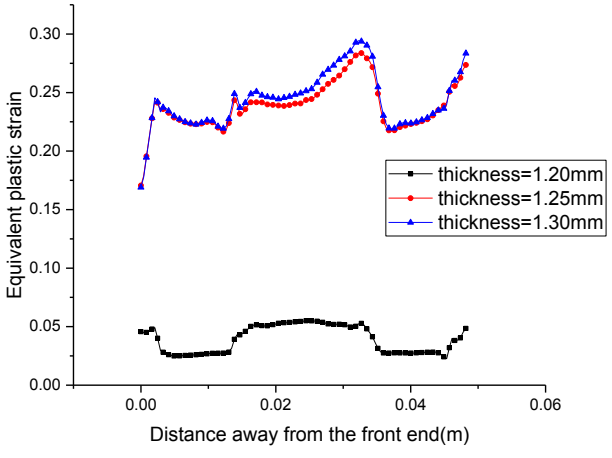

(c)

Fig. 5. The distribution of a) the maximum contact pressure, b) the through-thickness displacements along the path on coupon and c) the equivalent plastic strain on the cover.

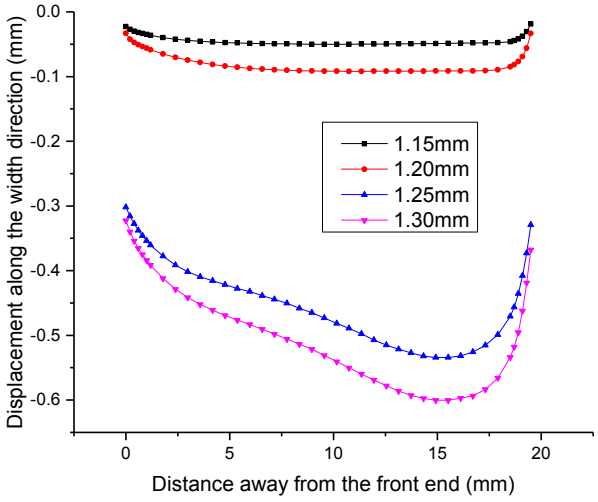

(b)

Fig. 7. The distribution of a) the maximum contact pressure and b) the width-direction displacement along the path in Fig. 6.

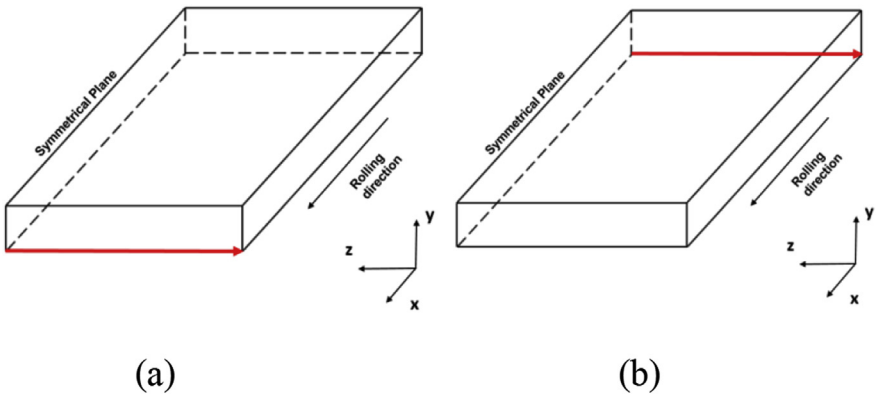

Fig. 8. The path along (a) the front surface, (b) the back surface.

mechanism and mechanical properties of the fuel coupon. As mentioned previously, the ideal elastic-plastic constitutive relation is adopted for UMo, and the fuel coupon will be squeezed to the gap between the cover and the frame. When the initial coupon thickness is enlarged, the fuel coupon will flow into these gaps and will not help for increase of the contact pressures.

The main purpose with a fuel coupon designed to be thicker than the frame lies in the idea that the bonding strength between the fuel coupon and the frame tends to be improved. In the following, the contact pressures will be given to compare the results for the four cases with different initial thicknesses of fuel coupon. A path in Fig. 6 is selected as the output path for the numerical results of contact pressures between the fuel coupon and the frame. The contact pressures and through-width displacement components are denoted in Fig. 7.

One can see from Fig. 7 (a) that the maximum contact pressures also increase with the initial values of coupon thickness. It can be observed that the maximum contact pressures of 1.25 mm-case and 1.30 mm-case are much larger than those of 1.15 mm-case and 1.20 mm-case, and the difference might reach about 100 MPa. Hence, the bonding strength at the formed interface between the fuel coupon and the frame can be effectively enhanced with a thicker fuel coupon designed. One can also find that the contact pressures near the two ends are lower than those at the other locations, which will induce weaker bonding strength there. The distribution characteristics of maximum contact pressures are similar respectively for 1.15 mm-case and 1.20 mm-case, and the same distribution pattern exists for 1.25 mm-case and 1.30 mm-case. While the distributions of contact pressures are of difference between 1.15mm/1.20 mm cases and 1.25mm/1.30 mm cases, which results from the induced different mechanical interactions among the fuel coupon, the cover and the frame. From Fig. 7 (b) one can find that the deformation patters of the fuel coupon along the width direction also present differences for 1.15mm/1.20 mm cases and 1.25mm/1.30 mm cases. For the 1.25mm/1.30 mm cases, similar dog-bone deformation characteristics appear. Induced by rolling, the fuel coupon is squeezed towards the tail end to form a dog-bone shape along the width direction.

The contact pressures at the front and back surfaces are also concerned. Two paths in Fig. 8 are selected to output the numerical simulation results. The distributions of the maximum contact pressure are shown in Fig. 9.

In can be found that the maximum contact pressures at the front surface could be about 20–40 MPa higher than those at the back surface, and they all rise with the initial thickness of fuel coupon. Compared with the maximum values of contact pressures for the 1.15 mm-case, the maximum values of 1.20 mm-case, 1.25 mm-case

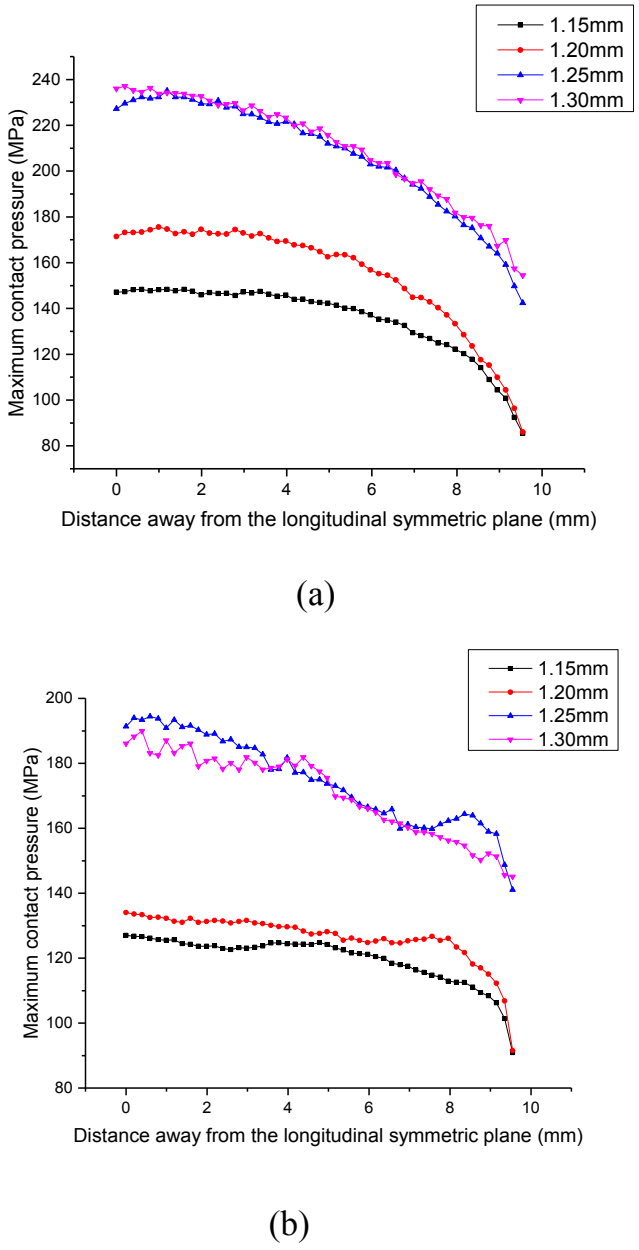

Fig. 9. The maximum contact pressures along (a) the front surface, (b) the back surface.

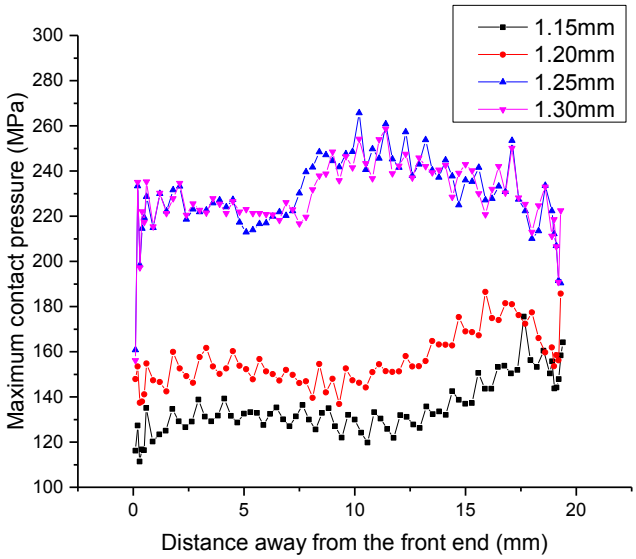

Fig. 10. The distribution of the maximum contact pressure along the central line.

and 1.30 mm-case are 16.56%, 54.51% and 60.52% higher at the front surface, and become 5.53%, 50.66% and 46.51% higher at the back surface. Similarly, the results for 1.25 mm-case and 1.30 mm-case are close to each other. It can be predicted that the formed interface at the front surface will have higher bonding strength, which relates to the rolling direction, the material flowing direction and the mutual interactions among all the parts. According to the simulation results, it can be obtained that an initial coupon thickness of ~1.25 mm is appropriate. If an optimized value of initial coupon thickness needs to be determined, new numerical simulation for more cases should be implemented. In the references, the initial thickness of fuel coupon ranges from 1.2 mm to 1.3 mm [7].

3.2. The influences of mechanical properties of UMo coupon

Considering that the mechanical properties of UMo alloy depends on the mass fraction of Mo, the fuel coupon might be softer for some candidates. In this section, the numerical simulation results of contact pressures are presented for the cases with a softened fuel coupon, which means that its Young's modulus and yield strength are lower than the values given in Section 2. They are reset as 32 GPa and 20 MPa.

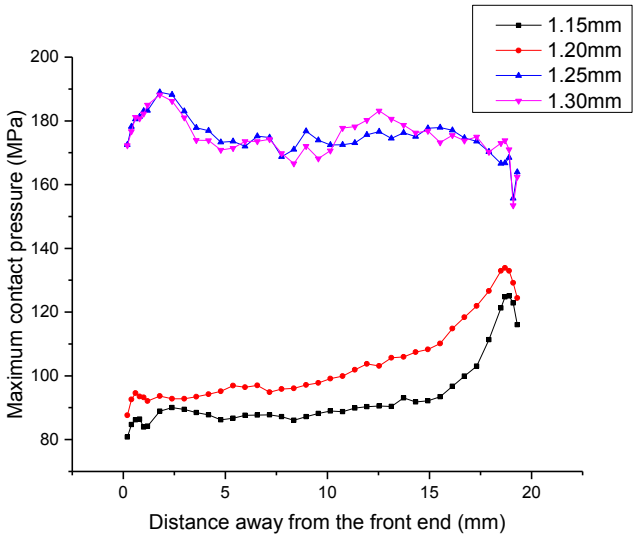

Fig. 11. The distribution of the maximum contact pressure along the path in Fig. 6.

The distribution of the maximum contact pressure along the path in Fig. 4 is shown in Fig. 10. The maximum contact pressure for 1.20 mm-case is about 20–40 MPa higher than those for 1.15 mm-case, and the maximum contact pressures for 1.25 mm-case and 1.30 mm-case are much higher, which could reach about 220–260 MPa.

The influence of the coupon thickness on the mechanical interaction between the fuel coupon and the frame could be seen in Fig. 11. The maximum contact pressures also rise with the initial coupon thickness, and the contact pressures for 1.25 mm-case and

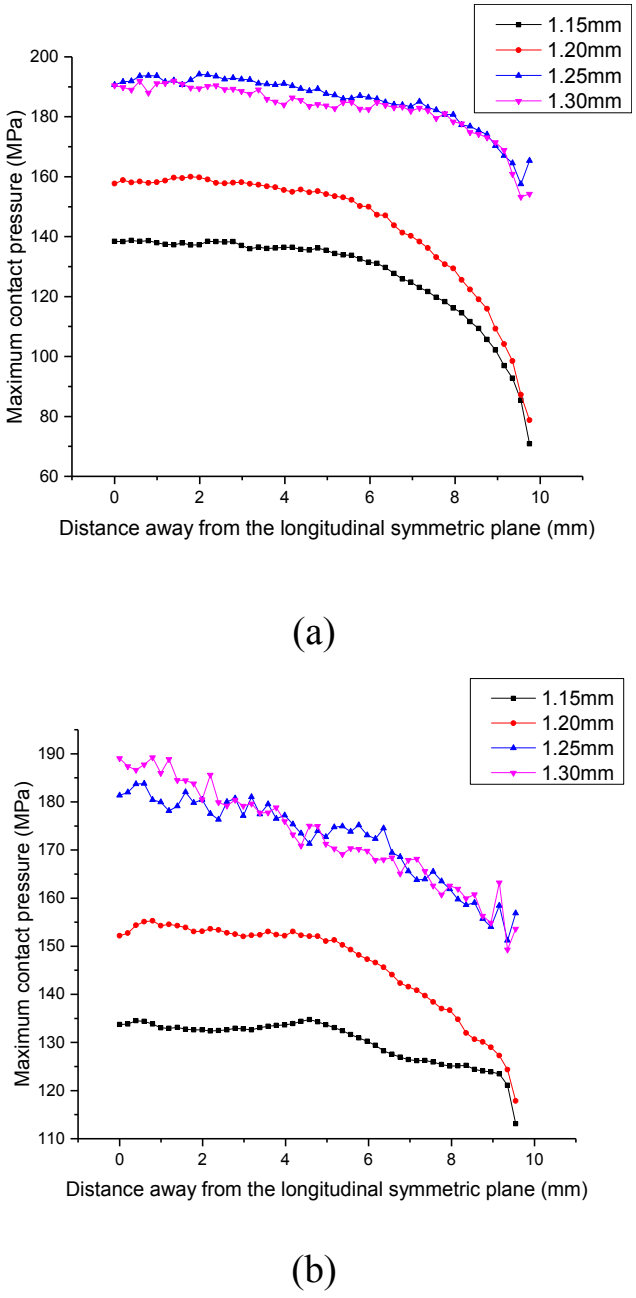

Fig. 12. The maximum contact pressure along (a) the front surface, (b) the back surface.

1.30 mm-case are nearly the same, which could be 80–100 MPa higher than those for 1.15 mm-case and 1.20 mm-case.

The maximum contact pressures at the front and back surfaces are shown in Fig. 12. One can also observe that it obeys the same rule as that in Section 3.1, but the contact pressure differences between the 1.15mm/1.20 mm cases and 1.25mm/1.30 mm cases are smaller. Compared to the maximum contact pressures for 1.15 mm-case, the maximum values for 1.20 mm-case, 1.25 mm-case and 1.30 mm-case increase by 13.97%, 37.80% and 37.62% at the front surface, and increase by 13.80%, 35.59% and 41.38% at the back surface. One can find that the minimum contact pressures at the path end rises a lot for 1.25 mm-case and 1.30 mm-case as well, compared to those for 1.15 mm-case and 1.20 mm-case. The minimum value at the front surface is 70.87 MPa for 1.15 mm-case, 78.73 MPa for 1.20 mm-case, and 157.51 MPa for 1.25 mm-case. It can be obtained that the corresponding bonding strength can be improved altogether when the initial thickness of fuel coupon reaches 1.25 mm or a larger value.

In order to compare the rolling simulation results for the cases with different coupon materials, in Fig. 13 the maximum contact pressures and through-thickness displacements along the path in Fig. 4 are given. The coupon material with the mechanical properties given in Section 2 is called Material 1, and the softened coupon material used in this section is called Material 2. From Fig. 13 (a), one can see that the contact pressures for Material 2 are lower as a whole than those for Material 1. One can't judge the bonding strength of the formed interface by Material 1 and Material 2, because the relation of the contact pressure with the bonding strength relies on the two materials to form the interface. Nevertheless, the results in Fig. 13 (a) indicate that for Material 2 the bonding strength can be also enhanced with a thicker fuel coupon. One can also find for the two cases with an initial coupon thickness of 1.25 mm that the contact pressure distributions are different for Material 1 and Material 2. The simulation results of contact pressure for Material 2 are lower near the front end of the path, which will result in weaker bonding strength there. This is for the reason that the plastic flow of Material 2 is easy to occur.

Fig. 13(b) denotes the through-thickness displacements for the cases with different coupon materials. The displacement differences for the two materials can scarcely be found when the initial coupon thickness is set as 1.20 mm. While for the two cases with an initial coupon thickness of 1.25 mm, the difference between the maximum thickness and minimum thickness after co-rolling is larger for Material 2, which indicates that a softened fuel coupon will appear to form an interface being more out-of-flatness. This results from the fact that with the same roller gap larger plastic deformation is easy to occur for a softer and thicker fuel coupon, so that the coupon part can easily flow towards the back end. In the in-pile environments, compared to the results at the flat interface, the interfacial stresses induced by the fuel swelling and creep will present some differences at the curved interface, which will possibly become a mechanism of interface fracture. As a result, the U-Mo alloy used as the fuel coupon should not be too soft.

4. Conclusions

In this study, co-rolling simulation results for a series of cases considering different values of initial coupon thickness have been obtained and investigated. The effects of mechanical properties of fuel coupon are also discussed. The conclusions are drawn as follows.

1) The maximum contact pressures between the fuel coupon and the Zircaloy cover exist near the central line, and decrease toward the edges along the plate width direction as a whole. Lower pressures occur at a large area near the corners of the fuel coupon, where the interfaces formed by the coupon and the cladding are easy to engender de-bonding in the in-pile irradiation environments.
2) The contact pressures between the U-Mo coupon and the Zircaloy parts rise remarkably when the initial thickness of the coupon increases, so increase of the initial coupon thickness could enhance the bonding strength after co-rolling. The contact pressures with a softened fuel coupon will be lower than those with a fuel coupon having higher elastic modulus and yield strength. A softened fuel coupon will appear to form an interface being more out-of-flatness, so the U-Mo alloy used as the fuel coupon should not be too soft.
3) When the initial coupon thickness increases to a certain value, further increase will affect the as-fabricated bonding strength

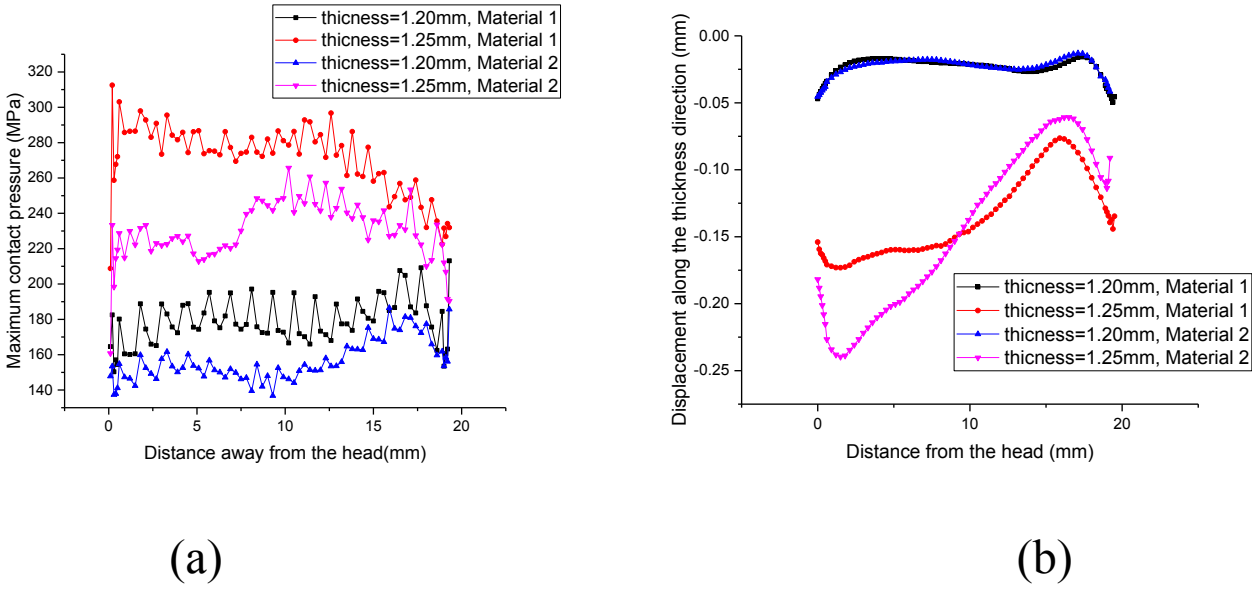

Fig. 13. a) The maximum contact pressure and b) the through-thickness displacement for the two kind UMo materials.

slightly. Thus, an optimized initial coupon thickness should be designed.

Acknowledgements

The authors thank for the supports of National Natural Science Foundation of China (No. 11572091, 11772095), the support of the National Key Research and Development Program of China (2016YFB0700103), and the support of the foundation from Science and Technology on Reactor System Design Technology Laboratory.

References

[1] H. Ozaltun, M.H. Shen, P. Medvedev, Assessment of residual stresses on U10Mo alloy based monolithic mini—plates during hot isostatic pressing, J. Nucl. Mater. 419 (1–3) (2011) 76–84.
[2] Y. Zhao, X. Gong, S. Ding, Simulation of the irradiation-induced thermo-mechanical behaviors evolution in monolithic U–Mo/Zr fuel plates under a heterogeneous irradiation condition, Nucl. Eng. Des. 285 (2015) 84–97.
[3] J.F. Jue, D.D. Keiser Jr., C.R. Breckenridge, et al., Microstructural characteristics of HIP-bonded monolithic nuclear fuels with a diffusion barrier, J. Nucl. Mater. 448 (1–3) (2014) 250–258.
[4] M.K. Meyer, J. Gan, J.F. Jue, et al., Irradiation performance of U-Mo monolithic fuel, Nucl. Eng. Technol. 46 (2) (2014) 169–182.
[5] Y. Park, J. Yoo, K. Huang, et al., Growth kinetics and microstructural evolution during hot isostatic pressing of U-10 wt.% Mo monolithic fuel plate in AA6061 cladding with Zr diffusion barrier, J. Nucl. Mater. 447 (1–3) (2014) 215–224.
[6] D.A. Lopes, A.J.O. Zimmermann, S.L. Silva, J.R.C. Piqueira, Thermal cycling effect in U-10Mo/Zry-4 monolithic nuclear fuel, J. Nucl. Mater. 473 (2016) 136–142.
[7] D. Keiser, F. Rice, CNEA Fresh Fuel Plate Characterization Summary Report, Idaho National Laboratory (INL), 2012.
[8] H.D. Manesh, H.S. Shahabi, Effective parameters on bonding strength of roll bonded Al/St/Al multilayer strips, J. Alloy. Comp. 476 (1–2) (2009) 292–299.
[9] H.Z. Yan, J.G. Lenard, A study of warm and cold roll-bonding of an aluminium alloy, Mater. Sci. Eng., A 385 (1–2) (2004) 419–428.
[10] N. Bay, Cold pressure welding—the mechanisms governing bonding, J. Eng. Ind. 101 (2) (1979).
[11] N. Bay, C. Clemensen, O. Juelstorp, T. Wanheim, Bond strength in cold roll bonding, CIRP Ann. - Manuf. Technol. 34 (1) (1985) 221–224.
[12] M. Abbasi, M.R. Toroghinejad, Effects of processing parameters on the bond strength of Cu/Cu roll-bonded strips, J. Mater. Process. Technol. 210 (3) (2010) 560–563.
[13] R. Jammaati, M.R. Toroghinejad, Investigation of the parameters of the cold roll bonding (CRB) process, Mater. Sci. Eng. 527 (9) (2010) 2320–2326.
[14] G. Zhou, L. Hua, D. Qian, et al., Effects of axial rolls motions on radial–axial rolling process for large-scale alloy steel ring with 3D coupled thermo-mechanical FEA, Int. J. Mech. Sci. 59 (1) (2012) 1–7.
[15] J.P. Hambleton, A. Drescher, On modeling a rolling wheel in the presence of plastic deformation as a three- or two-dimensional process, Int. J. Mech. Sci. 51 (11–12) (2009) 846–855.
[16] K. Ärölä, R. von Hertzen, Development of sheet tension under a rolling nip on a paper stack, Int. J. Mech. Sci. 47 (1) (2005) 110–133.
[17] Z. Zhuang, X.C. You, J.H. Liao, et al., Finite Element Analysis and Application Based on ABAQUS, Tsinghua University Press, Beijing, 2009.
[18] D.L. Hagrman, G.A. Reyman, MATPRO-Version11, A Handbook of Materials, Properties for use in the analysis of light water reactor fuel rod behavior, NUREG/CR-0497, TREE-1280, 1979, Rev.3.
[19] J. Wan, X. Kong, S. Ding, et al., Numerical simulation research on rolling process of monolithic nuclear fuel plate, Atomic Energy Sci. Technol. 49 (3) (2015) 511–517.
[20] X. Kong, H. Yang, S. Ding, Zircaloy plate rolling simulation with an effective strain-rate-dependent stress-updating algorithm, Int. J. Nonlinear Sci. Numer. Stimul. 17 (2) (2016) 113–125.